An Example of Computing the Failure-Tolerant Workspace Area for a Planar Kinematically Redundant Robot

P. S. Naik[+], *Student Member, IEEE*, A. A. Maciejewski[+], *Fellow, IEEE*, R. G. Roberts[*], *Senior Member, IEEE*, R. C. Hoover[†], *Member, IEEE*, and K. M. Ben-Gharbia[+], *Student Member, IEEE*

***Abstract*— Robots are frequently employed in structured environments for automating repetitive tasks. To extend their application to remote or hazardous environments, one must guarantee some measure of failure tolerance. One way to do this is to use kinematically redundant robots that have additional degrees of freedom. They are inherently robust to locked joint failures but the size of the reachable workspace after a failure depends on the design (and control) of the robot. The existence of such a workspace can be guaranteed by imposing a suitable set of artificial joint limits prior to a failure, however, this also limits the reachable pre-failure workspace. This work demonstrates how one can calculate an optimal tradeoff between pre-failure and post-failure workspace by determining the appropriate artificial joint limits. This is illustrated on a three degree-of-freedom planar robot generated from a PA-10 robot.**

I. INTRODUCTION [1]

Robots are frequently employed in structured environments for automating repetitive tasks. The goal of this work is to extend the use of robots to remote or hazardous environments, for example, in space exploration [3] and nuclear waste disposal [4], where failures are inevitable. The failure rates for components in such harsh environments are relatively high [5], [6], and maintenance is not possible. Many of these component failures will result in a robot's joint becoming immobilized, i.e., a locked joint failure mode, or be transformed into a locked joint by failure recovery mechanisms that employ fail safe brakes [7]. A number of studies have been dedicated to the assessment [8] and analysis [5], [9] of robot reliability. Other studies related to enhancing a robot's tolerance to failure include work on failure detection [10], layered failure tolerance control [11], failure tolerance by trajectory planning [12], kinematic failure recovery [13], and manipulators specifically designed for failure tolerance [14]. Because kinematically redundant robots have more joints than are required for a specified task, it is possible for such a robot to complete its assigned task even if it suffers a joint failure.

This work was supported in part by the National Science Foundation under Contract IIS-0812437.

[+]P. S. Naik, A. A. Maciejewski, and K. M. Ben-Gharbia are with the Department of Electrical and Computer Engineering, Colorado State University, Fort Collins, CO 80523-1373, USA {priya.naik, aam, khaled.ben-gharbia}@colostate.edu

[*]R. G. Roberts is with the Department of Electrical and Computer Engineering, College of Engineering, Florida A&M–Florida State University, Tallahassee, FL 32310-6046, USA rroberts@eng.fsu.edu

[†]R. C. Hoover is with the Department of Electrical and Computer Engineering, South Dakota School of Mines and Technology, Rapid City, SD 57701, USA randy.hoover@sdsmt.edu

[1]This paper builds on preliminary work described in [1] and [2].

One approach to guaranteeing failure tolerance is to add enough kinematic redundancy to compensate for a locked-joint failure [15]. It has been shown that by judiciously choosing suitable joint constraints, one can significantly increase the manipulator's failure-tolerant workspace, i.e., the guaranteed reachable pre- and post-failure workspace regardless of which joint fails, even if the manipulator only has one degree of redundancy. In [16], failure-tolerant workspaces that contain prescribed end-effector locations were identified by using bounding boxes in the configuration space that enclose self-motion manifolds corresponding to selected end-effector locations. In [1], [2], a theoretical framework was developed by the authors in which artificial joint limits are used to determine the boundaries of a failure-tolerant workspace. By imposing a set of artificial joint limits prior to failure, a suitable post-failure workspace can be developed. Once a joint has failed, it is locked in its current position for the remainder of the task. In this case, the artificial joint limits are released, and the remaining healthy joints are allowed to freely move within their physical joint limits.

The application of this approach has inherent tradeoffs. In particular, the tighter the artificial joint limits, the more the pre-failure workspace is reduced. In contrast, tighter artificial joint limits result in a greater guaranteed post-failure workspace. In this work, we illustrate how one can calculate an optimal tradeoff between pre-failure and post-failure workspace by determining the ideal artificial joint limits using bi-objective optimization. This is illustrated on a three degree-of-freedom planar robot generated from a PA-10 robot. We focus on the planar portion because it is easier to visualize. To extend our approach to a six-dimensional workspace one would need to apply techniques that are analogous to those in [17].

The remainder of this paper is organized as follows. The next section outlines the specific problem statement, i.e., how to determine the values of artificial joint limits that provide the desired pre- and post-failure workspaces for a given three degree-of-freedom robot. In section III we show how a brute force calculation can be performed to obtain the entire set of possible pre- and post-failure workspaces for an entire range of artificial joint limits. From this information one can identify the region of the design space where "optimal" sets of artificial joint limits exist, i.e., the Pareto optimal solutions. In the following two sections it is shown how the exact workspace boundary equations can be determined for a desired set of Pareto optimal solutions and then how they can

be integrated to obtain exact pre- and post-failure workspace areas. Finally, the conclusions of this work are presented in section VI.

II. PROBLEM FORMULATION

Assume that one is interested in operating a given robot in a locally fault tolerant manner [6] and in a manner that guarantees an optimal post-failure workspace. A planar three degree-of-freedom revolute (3R) robot is used here as an example. The forward kinematics of a planar 3R manipulator are given by

$$\mathbf{f}(\theta) = \begin{bmatrix} l_1\cos(\theta_1) + l_2\cos(\theta_{12}) + l_3\cos(\theta_{123}) \\ l_1\sin(\theta_1) + l_2\sin(\theta_{12}) + l_3\sin(\theta_{123}) \end{bmatrix} \quad (1)$$

where l_i is the length of link i, $\theta_{12} = \theta_1 + \theta_2$, and $\theta_{123} = \theta_1 + \theta_2 + \theta_3$. The local motion of the end effector is characterized by the Jacobian equation

$$\dot{\mathbf{x}} = J\dot{\mathbf{q}} \quad (2)$$

where $\dot{\mathbf{x}}$ denotes the end-effector velocity, $\dot{\mathbf{q}}$ denotes the vector of joint velocities, and J denotes the manipulator Jacobian. The canonical null vector of J, i.e., the null vector obtained by taking the equivalent of the cross product of the rows of J, is given by

$$\mathbf{n}_J = \begin{bmatrix} l_2 l_3 \sin(\theta_3) \\ -l_2 l_3 \sin(\theta_3) - l_1 l_3 \sin(\theta_2 + \theta_3) \\ l_1 l_2 \sin(\theta_2) + l_1 l_3 \sin(\theta_2 + \theta_3) \end{bmatrix}. \quad (3)$$

Note that $\mathbf{n}_J$ is not a function of θ_1. It has been previously shown [18] that an equal link length 3R manipulator has an optimally fault tolerant Jacobian at a configuration of $\theta^* = [0, 90^\circ, 90^\circ]^T$ as shown in Fig. 1. For the example presented here, we use the Mitsubishi PA-10-7C redundant manipulator, however, we lock joints 1, 3, 5, and 7 at zero degrees and then perform the analysis on the resulting planar 3R arm. The link lengths of the PA-10 are $l_1 = 0.45$ m, $l_2 = 0.5$ m, and $l_3 = 0.45$ m, where we have extended l_3 by a tool offset to make it equal to l_1. The range of the physical joint limits of the PA-10 are $\theta = [\pm 94^\circ, \pm 143^\circ, \pm 180^\circ]^T$, however to accommodate a tool extension the third joint limit is restricted to $\pm 150^\circ$. We analyze the guaranteed post-failure workspace for a range of artificial limits around this optimal configuration.

Let the kinematic function mapping the joint space $\boldsymbol{\mathcal{C}} \subset \mathbb{R}^n$ to the workspace $\boldsymbol{\mathcal{W}} \subset \mathbb{R}^m$ be denoted by $\mathbf{f} : \boldsymbol{\mathcal{C}} \to \boldsymbol{\mathcal{W}}$. In this work, we will assume that the configuration space $\boldsymbol{\mathcal{C}}$ has the form $\boldsymbol{\mathcal{C}_B} = B_1 \times \cdots \times B_n$ where $B_i = [\underline{b}_i, \bar{b}_i]$ represent the physical joint limits on joint i and $\underline{b}_i < \bar{b}_i$. If joint i has no physical joint limits then $B_i = \mathbb{R}$. Initially we introduce artificial limits for each joint so that the i^{th} joint $q_i \in [\underline{a}_i, \bar{a}_i]$ where $\underline{a}_i = \theta_i^* - \Delta\theta_i$ and $\bar{a}_i = \theta_i^* + \Delta\theta_i$ so that the artificial limits are symmetrically spaced around the optimal configuration θ^* by a value of $\Delta\theta$. Our initial experiments showed that symmetrical limits around the optimal point produce larger pre- and post-failure workspace areas as compared to non-symmetrical limits. If it can be safely assumed that joint i will not fail then one can set $[\underline{b}_i, \bar{b}_i] = [\underline{a}_i, \bar{a}_i]$.

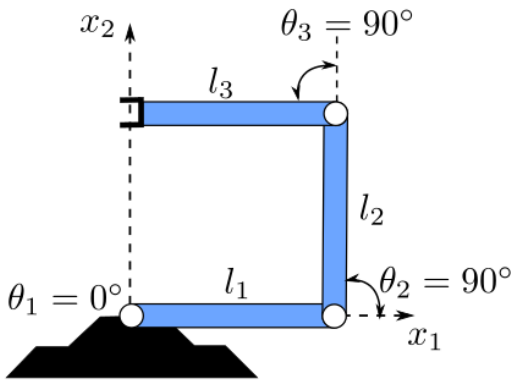

Fig. 1. A three link manipulator in the configuration $\theta = [0, 90^\circ, 90^\circ]^T$ that is optimally fault tolerant in a local sense. This robot is used as an example to show how one can compute the optimal tradeoff between pre-failure workspace and post-failure workspace by picking appropriate artificial joint limits.

The joint space prior to a failure is limited to the range of $[\underline{a}_i, \bar{a}_i]$ for all joints i. Once a locked-joint failure occurs, the artificial joint limits are released and the robot is constrained to operate on a failure-induced hyperplane. This of course has a significant impact on the resulting reachable workspace. There are generally end-effector locations that were reachable prior to the failure that are no longer reachable after a failure. There may also be areas of the workspace that were formerly unreachable but that, in spite of the locked joint, become reachable after releasing the artificial joint limits of the non-failed joints. The *fault tolerant workspace* is defined as the part of the workspace that is reachable prior to and after any single locked-joint failure where the joint failure can occur at any configuration within the artificially imposed joint limits $[\underline{a}_i, \bar{a}_i]$.

Prior to a joint failure, the robot's pre-failure workspace is given by

$$\boldsymbol{\mathcal{W}_0} = \{\mathbf{x} = \mathbf{f}(\mathbf{q}) \mid q_i \in [\underline{a}_i, \bar{a}_i] \forall i\}. \quad (4)$$

If the i^{th} joint is locked at $q_i = \theta_i$ and the remaining artificial joint limits are released, the resulting reduced configuration space is given by

$${}^i\boldsymbol{\mathcal{C}}(\theta_i) = \{\mathbf{q} \in \boldsymbol{\mathcal{C}_B} \mid q_i = \theta_i\}. \quad (5)$$

Geometrically, one can consider ${}^i\boldsymbol{\mathcal{C}}(\theta_i)$ to be the intersection of the hyperplane given by $q_i = \theta_i$ with the feasible configuration space $\boldsymbol{\mathcal{C}_B}$. Because the artificial joint limits were enforced prior to the failure, we have that $\underline{a}_i \leq \theta_i \leq \bar{a}_i$. It is assumed that the failure can occur anywhere in this interval and the joint is locked at that configuration. Hence, the guaranteed workspace following a locked-joint failure of joint i subject to the artificial joint limits is

$$\boldsymbol{\mathcal{W}_i} = \bigcap_{\underline{a}_i \leq \theta_i \leq \bar{a}_i} \mathbf{f}({}^i\boldsymbol{\mathcal{C}}(\theta_i)). \quad (6)$$

The fault tolerant workspace is then the intersection of the pre-failure workspace $\boldsymbol{\mathcal{W}_0}$ and the various post-failure fault tolerant workspaces $\boldsymbol{\mathcal{W}_i}$, $i \in \mathbf{F}$ where the *failure index set* $\mathbf{F} \subset \{1, 2, \ldots, n\}$ denotes the joint labels of the failure-prone joints, i.e.,

$$\boldsymbol{\mathcal{W}_F} = \boldsymbol{\mathcal{W}_0} \cap \left(\bigcap_{i \in F} \boldsymbol{\mathcal{W}_i} \right). \tag{7}$$

It can be seen that in order to ensure a failure tolerant workspace $\boldsymbol{\mathcal{W}_F}$, one needs to introduce artificial limits before a failure occurs. However, this constrains the pre-failure workspace $\boldsymbol{\mathcal{W}_0}$. This results in a classic case of two competing objectives where one must perform a bi-objective optimization to obtain the best possible pre-failure *and* post-failure workspace areas. Because there is an inherent tradeoff between these objectives whose optimal solution is dependent on the application, our goal is to provide flexibility to a designer by providing a set of "optimal" solutions depending on the relative importance of pre- and post-failure performance, i.e., we seek a set of Pareto optimal solutions. We denote the area of $\boldsymbol{\mathcal{W}_F}$ with A_F and the area of $\boldsymbol{\mathcal{W}_0}$ with A_0 and set as our objective the simultaneous maximization of the normalized versions of these areas, i.e., A_F/A_0 versus A_0/A_{0max}, where A_{0max} is the pre-failure workspace area without any artificial limits. The next section will discuss the computation of Pareto optimal solutions.

III. A Brute Force Technique for Computing Pareto Optimal Solutions

As the first step to computing a set of Pareto optimal solutions to our bi-objective optimization, we performed a brute force calculation to determine how the pre- and post-failure workspace, $\boldsymbol{\mathcal{W}_0}$ and $\boldsymbol{\mathcal{W}_F}$, vary as a function of the symmetric artificial joint limits. To this end, we discretized the two-dimensional workspace into a grid and for each grid square we computed the self-motion manifold [19], [20] of all possible configurations for our robot to reach that location.[2] We check whether the self-motion manifold for each grid square satisfies the conditions for membership in $\boldsymbol{\mathcal{W}_0}$ and $\boldsymbol{\mathcal{W}_i}$. These conditions are given below [1].

Condition for membership in $\boldsymbol{\mathcal{W}_0}$

A point $\mathbf{x} \in \boldsymbol{\mathcal{W}_0}$ if and only if there exists a self-motion manifold $\boldsymbol{\mathcal{M}_k}$ corresponding to $\mathbf{x}$ such that for $\mathbf{q} \in \boldsymbol{\mathcal{M}_k}$, $\underline{a}_i \leq q_i \leq \overline{a}_i$, for $i = 1, \ldots, n$.

Condition for membership in $\boldsymbol{\mathcal{W}_i}$, where $i \in \mathbf{F}$

A point $\mathbf{x} \in \boldsymbol{\mathcal{W}_i}$ if and only if there exists a union of self-motion manifolds $\boldsymbol{\mathcal{M}_k}$ corresponding to $\mathbf{x}$ whose projection onto the i^{th} axis completely covers the range $[\underline{a}_i, \overline{a}_i]$ with $\underline{b}_j \leq \theta_j \leq \overline{b}_j$ for $j = 1, \ldots, n$ and $j \neq i$.

A grid square that satisfies the first condition for $\boldsymbol{\mathcal{W}_0}$ and second condition for $\boldsymbol{\mathcal{W}_i}$ for all $i \in \mathbf{F}$ belongs to the failure tolerant workspace $\boldsymbol{\mathcal{W}_F}$. The number of squares satisfying these two conditions become our estimates of A_0 and A_F, respectively. Clearly, the accuracy of these approximate area calculations increases at a higher grid resolution. The results of these calculations for a wide range of artificial joint limits, i.e., $[5°, 5°, 5°] \leq \Delta\theta \leq [90°, 50°, 60°]$ with a step size of $5°$, are shown in Fig. 2 with a normalized version in Fig. 3. A portion of the Pareto optimal points that lie on the Pareto front are indicated with a red '*'. Clearly, these solutions represent different "optimal" values of the artificial joint limits for a range of different applications where the importance of pre-failure workspace area versus post-failure area varies. For the sake of illustration, assume that one is equally interested in both of these normalized areas. Therefore, one would be particulary curious about the region indicated in blue where $A_F/A_0 \approx A_0/A_{0max} \approx 0.2$. We show in the next section how one would exactly determine the equations for these workspace boundaries and thus compute exact values for these areas.

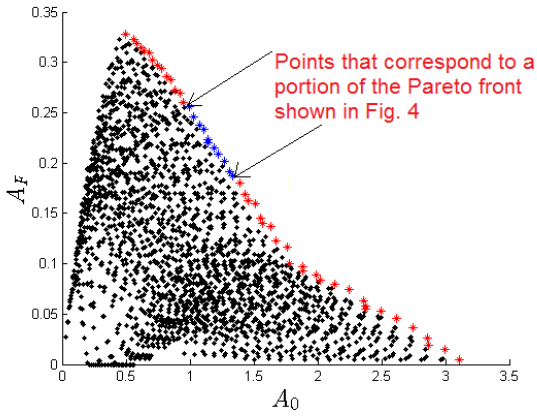

Fig. 2. Brute force analysis of the tradeoff between pre-failure workspace area A_0 and failure tolerant workspace area A_F over a range of artificial limits around the optimal configuration. The boundary points of this plot, indicated in red, represent Pareto optimal solutions, i.e., they represent solutions with the "best" tradeoff between A_0 and A_F.

IV. Computing Actual Boundary Equations

The brute force technique is a discretized version of the workspace and so the accuracy of the area computation depends on the resolution of the grid. An accurate calculation is possible by integrating over the actual boundary equations of the workspace. The equations for the boundary curves can be found by checking the self-motion manifold for a grid square just inside and outside of each workspace boundary to determine which condition is being violated. The above technique was used for points on the Pareto front and it was found that the boundary curves of $\boldsymbol{\mathcal{W}_0}$ and $\boldsymbol{\mathcal{W}_F}$ do not change for a portion of the Pareto front from $\Delta\theta = [23.3°, 44.2°, 39.9°]$ to $\Delta\theta = [29.9°, 50.6°, 46.8°]$.

This portion of the Pareto front is shown in Fig. 4. The boundary curves for $\boldsymbol{\mathcal{W}_0}$ and $\boldsymbol{\mathcal{W}_F}$ for a point $\Delta\theta = [24.4°, 45.1°, 40.9°]$ that falls within this range are shown in Figs. 5 and 6 respectively. The details of these three points are shown in the Table I. The constraint equations of these

[2]The complexity of computing the self-motion manifold increases dramatically with an increase in the degree of redundancy. One would need to employ a technique similar to that described in [16].

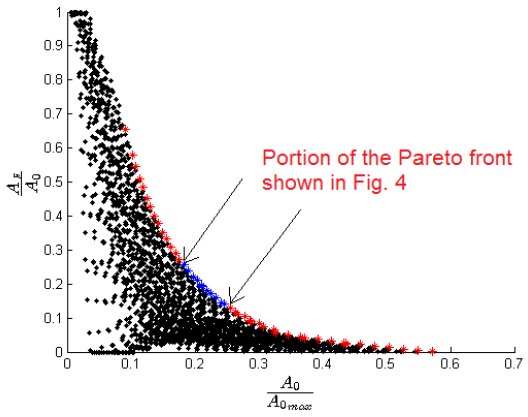

Fig. 3. Brute force analysis of the tradeoff between pre-failure workspace area A_0/A_{0max} and failure tolerant workspace area A_F/A_0 over a range of artificial limits around the optimal configuration. The points indicated in red represent a set of Pareto optimal solutions, i.e., they represent solutions with the "best" tradeoff between A_0/A_{0max} and A_F/A_0.

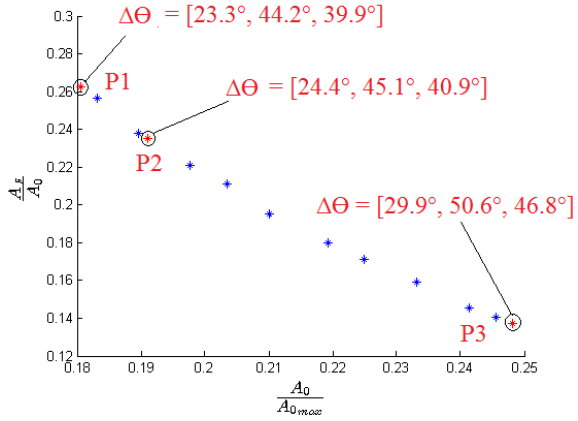

Fig. 4. Part of the Pareto front near the area of interest, i.e., $A_F/A_0 \approx A_0/A_{0max} \approx 0.2$, over which the boundary curves for $\boldsymbol{\mathcal{W}_0}$ and $\boldsymbol{\mathcal{W}_F}$ do not change.

boundaries are obtained by substituting the corresponding values of θ_i given in Tables II and III in the forward kinematic equation given by (1). The boundary condition satisfied by each curve is also given in the tables. These conditions are explained in [1]. Each curve is a circular arc with two of the joint angles having a constant value whereas the third is variable within a range. The range is determined by the joint angle values of the intersection point. The notation used for expressing a specific joint angle value i for a specific curve j is ${}^j\theta_i$. The notation used at a specific intersection point is as follows. Let j and k be two intersecting boundary curves and we are using the constraint equation of curve j to find the value of its variable joint i at the intersection point. This joint value is denoted by ${}^j_k\theta_i$. Similarly if we use the constraint equation of curve k to find the value of its variable joint i' at the same intersection point, this value is denoted by ${}^k_j\theta'_i$. Physically these joint values belong to two points that map to the same intersection point in the workspace, but in the configuration space they are two separate points on the same self motion manifold. Examples of the equations for computing the joint values at the intersection points are shown in the appendix.

V. Computing the Workspace Areas using Green's Theorem

Once the equations of the workspace boundaries are known, one can integrate over these curves to obtain the area of $\boldsymbol{\mathcal{W}_0}$ and $\boldsymbol{\mathcal{W}_F}$ by using Green's theorem [21], [22], i.e., given a region $D \subset \mathbb{R}^2$ bounded by a closed curve C,

$$g_A(D) = \int\int_D dA = \frac{1}{2}\int_C (x_1\, dx_2 - x_2\, dx_1) \qquad (8)$$

where $g_A(D)$ is the area of the region D. For computing the area of a workspace the closed loop C is a set of adjoining curves that form a closed loop. The workspace area is the sum of the areas under each curve computed in a counterclockwise direction over the loop. Consider a

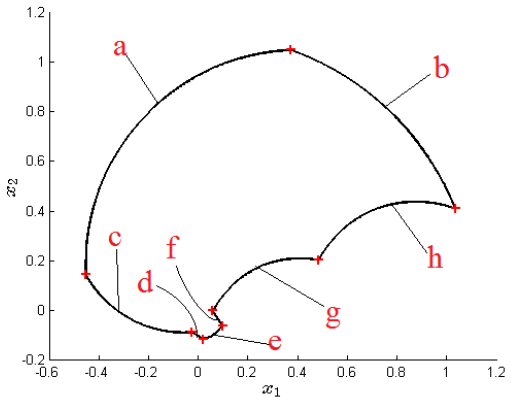

Fig. 5. Pre-failure workspace $\boldsymbol{\mathcal{W}_0}$ for $\Delta\theta_1 = 24.4°$, $\Delta\theta_2 = 45.1°$ and $\Delta\theta_3 = 40.9°$.

particular curve j with joint index i variable in its constraint equation. For such a curve, the workspace coordinates x_1 and x_2 are given as follows

$$x_1 = f_1(\theta_i) \qquad (9)$$
$$x_2 = f_2(\theta_i) \qquad (10)$$

where $\mathbf{f}$ is the forward mapping function given by (1) and θ_i is the variable joint. Therefore, Green's equation to compute area A_j under each curve j is of the form

$$A_j = \frac{1}{2}\int_{\theta_i} (f_1(\theta_i)\, df_2(\theta_i) - f_2(\theta_i)\, df_1(\theta_i))$$
$$= \frac{1}{2}\int_{\theta_i} \left(\left[f_1(\theta_i)\frac{df_2(\theta_i)}{d\theta_i} - f_2(\theta_i)\frac{df_1(\theta_i)}{d\theta_i} \right] d\theta_i \right). \qquad (11)$$

An example of the computations associated with this integration is given in the appendix.

The equation for the area of $\boldsymbol{\mathcal{W}_0}$ in Fig. 5 is then given by

$$A_0 = \sum_{j\in\{a,..,h\}} A_j \qquad (12)$$

TABLE I

DETAILS OF THE POINTS ON THE PARETO FRONT SHOWN IN FIG. 4

Point	$\Delta\theta$ (in degree)	A_0	A_F	$A_0/A_{0_{max}}$	A_F/A_0
$P1$	$[23.3°, 44.2°, 39.9°]$	0.9408	0.2333	0.1729	0.2480
$P2$	$[24.4°, 45.1°, 40.9°]$	0.9932	0.2223	0.1826	0.2239
$P3$	$[29.9°, 50.6°, 46.8°]$	1.3030	0.1600	0.2395	0.1228

TABLE II

BOUNDARIES FOR $\boldsymbol{\mathcal{W}_0}$.

Curve	θ_1	θ_2	θ_3	Boundary Condition Satisfied
a	$0 + \Delta\theta_1$	$\frac{\pi}{2} - \Delta\theta_2$ to $\frac{\pi}{2} + \Delta\theta_2$	$\frac{\pi}{2} - \Delta\theta_3$	$q_1 = \bar{a}_1$ and $q_3 = \underline{a}_3$
b	$0 - \Delta\theta_1$ to $0 + \Delta\theta_1$	$\frac{\pi}{2} - \Delta\theta_2$	$\frac{\pi}{2} - \Delta\theta_3$	$q_2 = \underline{a}_2$ and $q_3 = \underline{a}_3$
c	$0 + \Delta\theta_1$	$\frac{\pi}{2} + \Delta\theta_2$	$\frac{\pi}{2} - \Delta\theta_3$ to ${}^{c}_{d}\theta_3$	$q_1 = \bar{a}_1$ and $q_2 = \bar{a}_2$
d	$0 - \Delta\theta_1$	$\frac{\pi}{2} + \Delta\theta_2$	${}^{d}_{c}\theta_3$ to $\frac{\pi}{2} + \Delta\theta_3$	$q_1 = \underline{a}_1$ and $q_2 = \bar{a}_2$
e	$0 - \Delta\theta_1$ to $0 + \Delta\theta_1$	$\frac{\pi}{2} + \Delta\theta_2$	$\frac{\pi}{2} + \Delta\theta_3$	$q_2 = \bar{a}_2$ and $q_3 = \bar{a}_3$
f	$0 + \Delta\theta_1$	${}^{f}_{g}\theta_2$ to $\frac{\pi}{2} + \Delta\theta_2$	$\frac{\pi}{2} + \Delta\theta_3$	$q_1 = \bar{a}_1$ and $q_3 = \bar{a}_3$
g	$0 - \Delta\theta_1$	$\frac{\pi}{2} - \Delta\theta_2$ to ${}^{g}_{f}\theta_2$	$\frac{\pi}{2} + \Delta\theta_3$	$q_1 = \underline{a}_1$ and $q_3 = \bar{a}_3$
h	$0 - \Delta\theta_1$	$\frac{\pi}{2} - \Delta\theta_2$	$\frac{\pi}{2} - \Delta\theta_3$ to $\frac{\pi}{2} + \Delta\theta_3$	$q_1 = \underline{a}_1$ and $q_2 = \underline{a}_2$

TABLE III

BOUNDARIES FOR $\boldsymbol{\mathcal{W}_F}$.

Curve	θ_1	θ_2	θ_3	Boundary Condition satisfied
p	$0 - \Delta\theta_1$	$\bar{b}_2$	0 to $\frac{\pi}{2} - \Delta\theta_3$	$q_1 = \underline{a}_1$ and $q_2 = \bar{b}_2$
q	$0 - \Delta\theta_1$	${}^{q}_{r}\theta_2$ to $\bar{b}_2$	0	$n_{J_1}(\mathbf{q}) = 0$ and $q_1 = \underline{a}_1$
r	${}^{r}_{q}\theta_1$ to ${}^{r}_{v}\theta_1$	$\frac{\pi}{2} + \Delta\theta_2$	$\arctan\left(\frac{l_1 \cos\Delta\theta_2}{l_1 \sin\Delta\theta_2 - l_2}\right)$	$n_{J_2}(\mathbf{q}) = 0$ and $q_2 = \bar{a}_2$
s	$\underline{b}_1$ to $0 - \Delta\theta_1$	$\bar{b}_2$	$\frac{\pi}{2} - \Delta\theta_3$	$q_2 = \bar{b}_2$ and $q_3 = \underline{a}_3$
t	$\underline{b}_1$	${}^{t}_{u}\theta_2$ to $\bar{b}_2$	$\frac{\pi}{2} - \Delta\theta_3$	$q_1 = \underline{b}_1$ and $q_3 = \underline{a}_3$
u	$0 + \Delta\theta_1$	${}^{u}_{v}\theta_2$ to ${}^{u}_{t}\theta_2$	$\bar{b}_3$	$q_1 = \bar{a}_1$ and $q_3 = \bar{b}_3$
v	$0 - \Delta\theta_1$	$\frac{\pi}{2} - \Delta\theta_2$	${}^{v}_{r}\theta_3$ to ${}^{v}_{u}\theta_3$	$q_1 = \underline{a}_1$ and $q_2 = \underline{a}_2$

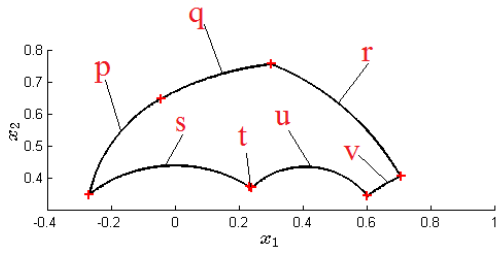

Fig. 6. Failure tolerant workspace $\boldsymbol{\mathcal{W}_F}$ for $\Delta\theta_1 = 24.4°$, $\Delta\theta_2 = 45.1°$ and $\Delta\theta_3 = 40.9°$

and the area of $\boldsymbol{\mathcal{W}_F}$ in Fig. 6 is given by

$$A_F = \sum_{j \in \{p,..,v\}} A_j \tag{13}$$

where A_j is the area associated with curve j belonging to either $\boldsymbol{\mathcal{W}_0}$ or $\boldsymbol{\mathcal{W}_F}$, respectively. An example of the computations associated with determining these areas is given in the appendix.

The above area equations allow one to exactly compute the optimal values of $A_0/A_{0_{max}}$ and A_F/A_0 for different points along the desired Pareto front. In practice, this would be used by an automation engineer who is applying a robot to perform a task in an environment that requires fault tolerance to select an optimal set of artificial joint limits for the robot's controller that would guarantee task completion even after a failure.

VI. CONCLUSION

This paper has considered the situation where an automation engineer is applying a robot to autonomously perform a task in a remote or hazardous environment where failures are inevitable. In order to maintain operation for as long as possible, one would like to make the robot tolerant to at least one joint failure. One technique for doing this is to use kinematic redundancy and impose artificial joint limits prior to a failure. However, the optimal value of these artificial joint limits involves a bi-objective optimization between two

competing factors, i.e., the available pre-failure workspace and the guaranteed post-failure workspace. This work shows how one can compute the entire range of optimal choices, i.e., Pareto optimal solutions, depending on the desired tradeoff between pre- and post-failure workspace. This was illustrated on a planar 3R robot obtained from considering three joints of the commercial PA-10 robot.

APPENDIX

This appendix presents examples of the equations required to compute the intersection points of the boundary equations that represent the limits of integration in (11), as well as the actual areas A_0 and A_F in (12) and (13).

A. Computing A_0

The first step in computing A_0 is to compute the limits of integration for the joint variable under consideration. For example, for boundary curve a in Fig. 5 the integration variable is θ_2 and its limits are given by

$$
\begin{aligned}
{}^{a}_{b}\theta_2 &= \frac{\pi}{2} - \Delta\theta_2 \quad \text{and} && (14)\\
{}^{a}_{c}\theta_2 &= \frac{\pi}{2} + \Delta\theta_2. && (15)
\end{aligned}
$$

Now we apply Green's theorem over the above computed ranges of integration for each curve in workspace $\boldsymbol{\mathcal{W}_0}$ in an anticlockwise sense to calculate (12). For example, the area associated with curve a is given by

$$
\begin{aligned}
A_a = \frac{1}{2}\Big[\pi\left({l_2}^2 + {l_3}^2\right) + 2\pi l_2 l_3 \sin(\Delta\theta_3) \\
-2 l_1 l_3 \sin(\Delta\theta_2)\cos(\Delta\theta_3)\Big]. \qquad (16)
\end{aligned}
$$

B. Computing A_F

A similar procedure is used to compute A_F. For example, the equations for the limits of integration on curve s are given by

$$
\begin{aligned}
{}^{s}_{p}\theta_1 &= -\Delta\theta_1 \quad \text{and} && (17)\\
{}^{s}_{t}\theta_1 &= \underline{b}_1. && (18)
\end{aligned}
$$

Once all the limits of integration are determined, one can calculate (13). For example, the area under curve s is given by

$$
\begin{aligned}
A_s = \frac{(\underline{b}_1 + \Delta\theta_1)}{2}\Big[{l_1}^2 + {l_2}^2 + {l_3}^2 + 2 l_1 l_2 \cos(\bar{b}_2) \\
+2 l_2 l_3 \sin(\Delta\theta_3) + 2 l_1 l_3 \sin(\Delta\theta_3 - \bar{b}_2)\Big]. \qquad (19)
\end{aligned}
$$

REFERENCES

[1] R. C. Hoover, R. G. Roberts, and A. A. Maciejewski, "Implementation issues in identifying the failure-tolerant workspace boundaries of a kinematically redundant manipulator," in *IEEE Int. Conf. on Intelligent Robots and Systems*, San Diego, CA, Oct 29- Nov 2 2007, pp. 3528 –3533.

[2] R. G. Roberts, R. J. Jamisola Jr., and A. A. Maciejewski, "Identifying the failure-tolerant workspace boundaries of a kinematically redundant manipulator," in *IEEE Int. Conf. Robot. Automat.*, Roma, Italy, April 10-14 2007, pp. 4517–4523.

[3] E. C. Wu, J. C. Hwang, and J. T. Chladek, "Fault-tolerant joint development for the space shuttle remote manipulator system: Analysis and experiment," *IEEE Trans. Robot. Automat.*, vol. 9, no. 5, pp. 675–684, Oct. 1993.

[4] R. Colbaugh and M. Jamshidi, "Robot manipulator control for hazardous waste-handling applications," *J. Robot. Syst.*, vol. 9, no. 2, pp. 215–250, 1992.

[5] B. S. Dhillon A. R. M. Fashandi and K. L. Liu, "Robot systems reliability and safety: A review," *J. Quality Maintenance Engineering*, vol. 8, no. 3, pp. 170–212, 2002.

[6] K. N. Groom, A. A. Maciejewski, and V. Balakrishnan, "Real-time failure-tolerant control of kinematically redundant manipulators," *IEEE Trans. Robot. Automat.*, vol. 15, no. 6, pp. 1109–1116, Dec. 1999.

[7] P. Nieminen, S. Esque, A. Muhammad, J. Mattila, J. Väyrynen, M. Siuko, and M. Vilenius, "Water hydraulic manipulator for fail safe and fault tolerant remote handling operations at ITER," *Fusion Engineering and Design*, vol. 84, no. 7, pp. 1420–1424, 2009.

[8] S. Tosunoglu and V. Monteverde, "Kinematic and structural design assessment of fault-tolerant manipulators," *Intell. Automat. Soft Comput.*, vol. 4, no. 3, pp. 261–268, 1998.

[9] C. Carreras and I. D. Walker, "Interval methods for fault tree analysis in robotics," *IEEE Trans. Robot. Automat.*, vol. 50, no. 1, pp. 3–11, Mar. 2001.

[10] L. Notash, "Joint sensor fault detection for fault tolerant parallel manipulators," *J. Rob. Syst.*, vol. 17, no. 3, pp. 149–157, 2000.

[11] Y. Ting, S. Tosunoglu, and B. Fernandez. "Control algorithms for fault-tolerant robots," *IEEE Int. Conf. Robot. Automat.*, vol. 2, pp. 910–915, May 8–13, 1994.

[12] S. K. Ralph and D. K. Pai, "Computing fault tolerant motions for a robot manipulator," in *IEEE Int. Conf. Robot. Automat.*, Detroit, MI, May 10-15 1999, pp. 486–493.

[13] J. Park, W.-K. Chung, and Y. Youm, "Failure recovery by exploiting kinematic redundancy," in *Proc. 5th Int. Workshop on Robot Human Commun*, Tsukuba, Japan, November 11-14 1996, pp. 298–305.

[14] Y. Yi, J. E. McInroy, and Y. Chen, "Fault tolerance of parallel manipulators using space and kinematic redundancy," *IEEE Trans. Robotics*, vol. 22, no. 5, pp. 1017–1021, Oct. 2006.

[15] C. J. J. Paredis and P. K. Khosla, "Designing fault-tolerant manipulators: How many degrees of freedom?" *Int. J. Robot. Res.*, vol. 15, no. 6, pp. 611–628, Dec. 1996.

[16] C. L. Lewis and A. A. Maciejewski, "Fault tolerant operation of kinematically redundant manipulators for locked joint failures," *IEEE Trans. Robot. Automat.*, vol. 13, no. 4, pp. 622–629, Aug. 1997.

[17] K. M. Ben-Gharbia, A. A. Maciejewski, and R. G. Roberts, "Kinematic Design of Redundant Robotic Manipulators for Spatial Positioning that are Optimally Fault Tolerant," accepted to appear in *IEEE Trans. Robot.*, 2013.

[18] R. G. Roberts and A. A. Maciejewski, "A local measure of fault tolerance for kinematically redundant manipulators," *IEEE Trans. Robotics Automat.*, vol. 12, no. 4, pp. 543–552, Aug. 1996.

[19] C. Lück, "Self-motion representation and global path planning optimization for redundant manipulators through topology based discretization," *J. Intel. Rob. Syst.*, vol. 19, no. 1, pp. 23–38, May 1997.

[20] J. Lenarčič, "Some considerations on the self motion curves of a planar 3R manipulator," *J. Computer Inform. Tech.*, vol. 10, no. 2, pp. 125–131, 2002.

[21] J. P. Merlet, C. M. Gosselin, and N. Mauly, "Workspaces of planar parallel manipulators," *Mech. Mach. Theory*, vol. 33, no. 1/2, pp. 7–20, 1998.

[22] C. Gosselin, "Determination of the workspace of 6-DOF parallel manipulators," *ASME J. Mech. Design*, vol. 112, no. 3, pp. 331–336, 1990.